ACS APPLIED MATERIALS & INTERFACES

Research Article

www.acsami.org

General Strategy for Fabricating Sandwich-like Graphene-Based Hybrid Films for Highly Reversible Lithium Storage

Xiongwu Zhong,[†] Zhenzhong Yang,[‡] Xiaowu Liu,[†] Jiaqing Wang,[†] Lin Gu,[‡] and Yan Yu*[,†,§]

[†]Key Laboratory of Materials for Energy Conversion, Chinese Academy of Sciences, Department of Materials Science and Engineering, University of Science and Technology of China, No. 96 Jinzhai Road, Hefei, Anhui 230026, P. R. China

[‡]Beijing National Laboratory for Condensed Matter Physics, The Institute of Physics, Chinese Academy of Sciences, Beijing 100190, P. R. China

[§]State Key Laboratory of Fire Science, University of Science and Technology of China, Hefei, Anhui 230026, P. R. China

Supporting Information

ABSTRACT: We report a general strategy for the fabrication of freestanding sandwich-like graphene-based hybrid films by electrostatic adsorption and following reduction reaction. We demonstrate that by rational control of pH value in precursors, graphene oxide (GO) sheets can form three-dimensional (3D) sandwich frameworks with nanoparticles decorated between the layers of graphene. In our proof-of-concept study, we prepared the graphene/Si/graphene (G@Si@G) sandwich-like films. When used as negative electrode materials for lithium-ion batteries, it exhibits superior lithium-ion storage performance (~1800 mA h g^{-1} after 40 cycles at 100 mA g^{-1}). Importantly, with this simple and general method, we also successfully synthesized graphene/Fe_2O_3/graphene and graphene/TiO_2/graphene hybrid films, showing improved electrochemical performance. The good electrochemical property results from the enhanced electron transport rate, and the 3D flexible matrix to buffer volume changes during cycling. In addition, the porous sandwich structure consisting of plate-like graphene with high surface area provides effective electrolyte infiltration and promotes diffusion rate of Li^+, leading to an improved rate capability.

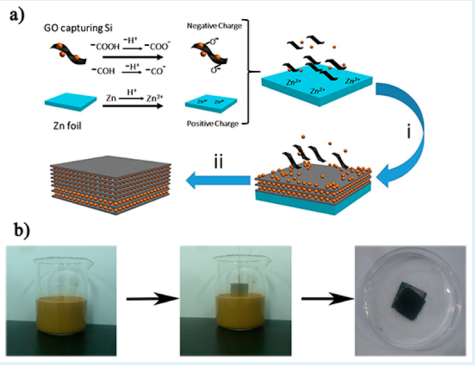

KEYWORDS: *lithium-ion batteries, graphene, sandwich structure, freestanding, anode*

1. INTRODUCTION

Over the past decade, many studies have developed for advanced lithium-ion batteries (LIBs) to meet the requirements of future portable electronics and electric vehicles (EVs).[1] To meet the increasing demand of high-performance LIBs, LIBs with high energy density should be prepared by advanced battery materials.[2] The IV group elemental materials (silicon, germanium, tin)[3] and transition metal oxides (M_xO_y such as Fe_2O_3)[4] have been studied to offer multiple times of specific lithium storage capacity of the commercial carbonaceous anodes and confirmed to be promising next generation battery electrodes. Nevertheless, the industrialized application of such materials has been frustrated by their low power rate and short cycle life resulting from the huge volume expansion in time of cycling, poor conductivity, and sluggish diffusivity for lithium ions.[5] Many strategies have been carried out to address those problems by introducing a protection layer, protecting the structures with surface conductive coatings (such as carbon coating), preparing nanosized materials, creating hybrid materials with porous structure.[6] It has been demonstrated that construction of buffer cushion could improve the rate performance of these materials resulting from enhancements of the mechanical strength, electrical conductivity between the electroactive material and the current collector, and the high lithium-ion diffusion. Another effective strategy is to design nanoscale hierarchical structure, which can alleviate the breakage of the electroactive materials. Moreover, smaller particle shortens the diffusion path of Li-ion and shows higher specific surface area, decreasing charge transfer resistance, finally furthering the electrochemical performance of electrode.[7]

Among the manifold strategies, the best choice is the designing of nanoscale hierarchical structure with carbon as a result of its unique chemical and physical properties and low price of carbon.[8] In addition, carbon could work as a protection layer to accommodate the huge volume expansion during cycling and lead to improved cycle performance. A variety morphology of carbon (i.e., CNT, porous carbon, graphene, carbon nanofibers) has been developed to composite with IV main group element and transition metal oxides, leading to significant improvements for cyclability and rate capability.[3,9] Among them, two-dimensional (2D) graphene shows ex-

Received: May 8, 2015
Accepted: August 10, 2015
Published: August 10, 2015

ACS Publications © 2015 American Chemical Society

DOI: 10.1021/acsami.5b03942
ACS Appl. Mater. Interfaces 2015, 7, 18320−18326

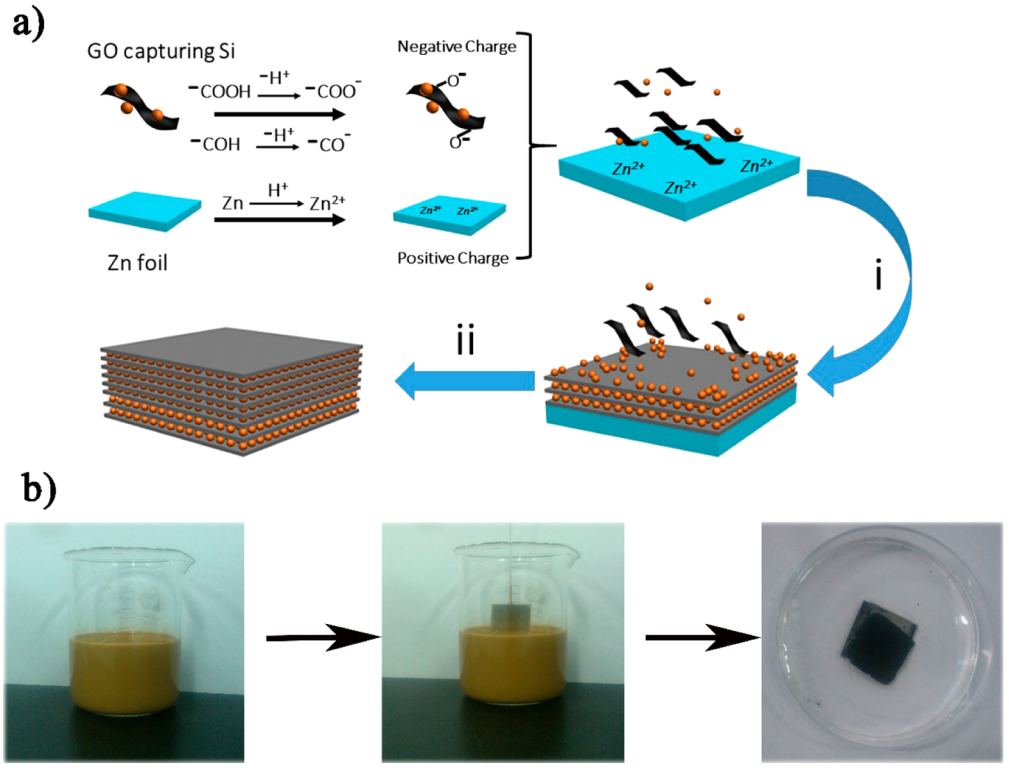

Figure 1. (a) Schematic illustration of the process for the graphene-based hybrid films: (i) self-assembly and interfacial gelation; (ii) detached from Zn foils. (b) The optical images of the process for the G@Si@G films.

tremely promising to improve the cycle performance and rate capability of the cell because of its advantages such as superior conductivity, wonderful mechanical flexibility, and high surface area.[10] As for graphene-based nanostructure, the sandwich-like structure can take the best use of the excellent characteristics of graphene. In general, there are two methods to preparing graphene-based sandwich-like structure: (i) nanoparticles were first loaded on the graphene, following by the carbon coating procedure;[11−14] (ii) the nanoparticles were mixed with graphene dispersion, then the sandwich-like structure was obtained by filtrating or drying the suspensions.[14,15] Moreover, to further enhance power density of batteries as well as simplify the cell packing process, it is an ideal strategy to fabricate a flexible, self-standing, and binder-free electrode, where all the materials could make contribution to lithium storage.[16]

Herein, we report a general strategy for synthesis of freestanding sandwich-like graphene-based hybrid films by electrostatic adsorption. The unique electrode architectures formed a three-dimensional (3D) graphene-based framework filled with nanometer-sized electroactive materials. In our proof-of-concept study, graphene/Si/graphene sandwich-like films (denoted as G@Si@G) were successfully demonstrated and displayed improved lithium storage properties when used as anode for LIBs.

2. EXPERIMENTAL SECTION

2.1. Materials Synthesis. Synthesis of carbon coated Si nanoparticles: the commercial Si nanoparticles were coated with carbon using a solvothermal process. Typically, 0.1 g of Si nanoparticles (Sigma-Aldrich Co. LLC), 8 g of glucose, and 1 g of poly(vinylpyrrolidinone) (PVP) were added into 40 mL of deionized water (DI); the mixture was sonicated until Si nanoparticles were homogeneously dispersed in the solution. Then the mixture was transferred to a Teflon-lined stainless-steel autoclave. After solvothermal treatment at 160 °C for 12 h, the product was collected after centrifugation, then three times thoroughly washed with DI, and finally dried at 75 °C in a vacuum oven.

Synthesis of Si@C nanoparticles: Si@C nanoparticles were obtained by via calcination process at 800 °C for 3 h under a 5% H_2/95% Ar atmosphere using carbon coated Si nanoparticles.

Synthesis of Fe_2O_3 nanoparticles: the Fe_2O_3 nanoparticles were prepared by a facile hydrothermal synthetic method.[17] In a typical procedure, 0.6 mmol $K_4Fe(CN)_6$, 30 mL of sodium carboxymethyl cellulose soluton (1.25g L^{-1}), 0.4 g of PVP, and 0.4 mL of N_2H_4 solution were added into a 40 mL of DI in a Teflon-line autoclave. Then the autoclave was kept at 200 °C for 6 h. The red precipitate was collected and washed with DI several times (see Figure S8).

Synthesis of the G@Si@G films: in a typical synthesis, 50 mg of carbon coated Si nanoparticles was added into 50 mL of aqueous GO dispersion (2 mg mL^{-1}). The pH of the mixture was adjusted to 2 using 1 M HCl aqueous solution. Then the suspensions were sonicated until carbon coated Si nanoparticles were homogeneously dispersed in the solution. After being hanged in the middle of the suspensions for 3 h at room temperature, Zn foils were taken out, and the hybrid films were detached to remove Zn substrate by mild acid etching and washed by pure water. After freeze-drying, the G@Si@G films were obtained via calcination process at 800 °C for 3 h under a 5% H_2/95% Ar atmosphere. The G@Si@G films with higher weight ratio of Si (H-G@Si@G films) were obtained by increasing the mass of Si nanoparticles to 75 mg.

Synthesis of G@Fe_2O_3@G films: in a typical synthesis, 150 mg of Fe_2O_3 nanoparticles was added into 50 mL of aqueous graphene oxide (GO) dispersion (2 mg mL^{-1}). The pH of the mixture was adjusted to 2 using 1 M HCl aqueous solution. Then the suspensions were sonicated until Fe_2O_3 nanoparticles were homogeneously dispersed in the solution. After being hanged in the middle of the suspensions for 3 h at room temperature, Zn foils were taken out, and the hybrid films were detached to remove Zn substrate by mild acid etching and washed by pure water. After freeze-drying, the G@ Fe_2O_3@G films were obtained via calcination process at 550 °C for 3 h under an Ar atmosphere.

DOI: 10.1021/acsami.5b03942
ACS Appl. Mater. Interfaces 2015, 7, 18320−18326

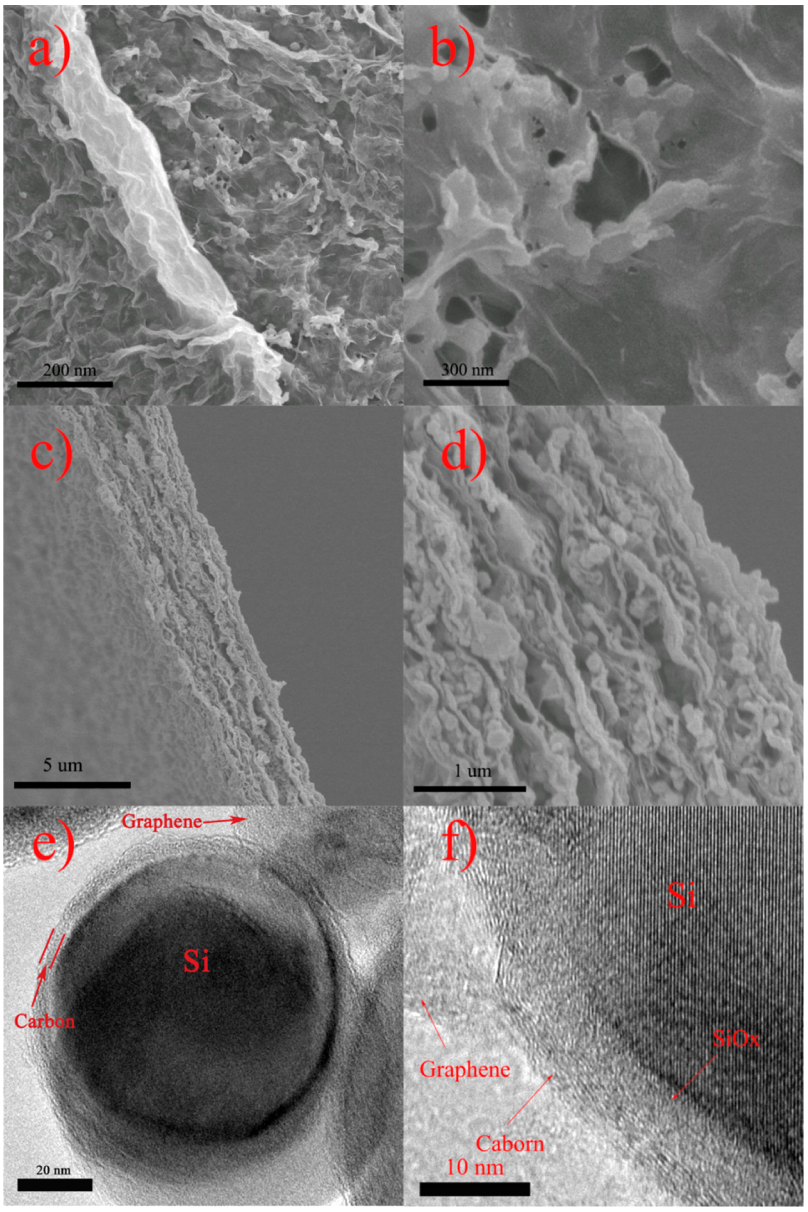

Figure 2. (a, b) SEM images of the surface of the G@Si@G films. (c, d) Cross-sectional SEM images of the G@Si@G films. (e, f) TEM and HRTEM images of the G@Si@G films, respectively.

Synthesis of G@TiO_2@G films: in a typical synthesis, 300 mg of commercial TiO_2 nanoparticles (Sigma-Aldrich Co. LLC) was added into 50 mL of aqueous GO dispersion (2 mg mL^{-1}). The pH of the mixture was adjusted to 2 using 1 M HCl aqueous solution. Then the suspensions were sonicated until TiO_2 nanoparticles were homogeneously dispersed in the solution. After being hanged in the middle of the suspensions for 3 h at room temperature, Zn foils were taken out, and the hybrid films were detached to remove Zn substrate by mild acid etching and washed by pure water. After freeze-drying, the G@TiO_2@G films were obtained via calcination process at 550 °C for 3 h under an Ar atmosphere.

2.2. Materials Characterization. X-ray diffraction (XRD) (TTR-III, Rigaku, Japan) using Cu Kα radiation was used to characterize the graphene-based hybrid films. The morphology and microstructure of the graphene-based hybrid films were characterized by A JEOL 4000EX transmission electron microscope (HRTEM) (JEOL, Tokyo, Japan), a JSM-6700 field-emission scanning electron microscope (JEOL, Tokyo, Japan) operated at 5 keV. As for elemental analysis, the Thermo-VG Scientific instrument was used for X-ray photoelectron spectroscopy (XPS) experiments. Thermogravimetric (TG) analysis (TGA Q5000 instrument) was measured at a heating rate of 10 K min^{-1} in air.

2.3. Electrochemical Characterization. The coin-type half-cells (CR2032) were assembled in an argon-filled glovebox. As for the Si@C nanoparticles electrodes, Si@C nanoparticles, carbon black, and poly(vinylidene fluoride) (PVDF) were mixing in a weight ratio of 80:10:10 and made into a slurry onto a copper foil. The freestanding films were cut into pieces with size 0.5 cm × 0.5 cm, and the masses of the G@Si@G, G@Fe_2O_3@G, and G@TiO_2@G films were about 0.6, 0.5, and 0.7 mg cm^{-2}, respectively. The electrolyte was 1 M $LiPF_6$ in ethylene carbonate (EC)/dimethyl carbonate (DEC) (1:1 = w/w), and separator is the celgard 2400 menbrane. Cyclic voltammetry (CV) measurements were performed on a CHI 660D electrochemical workstation (Chenhua Instrument Company, Shanghai, China) at a scan rate of 0.04 mV s^{-1}.

3. RESULTS AND DISCUSSION

Figure 1, panel a illustrates fabrication processes and resulting freestanding G@Si@G films. During a experiment process, Si

DOI: 10.1021/acsami.5b03942
ACS Appl. Mater. Interfaces 2015, 7, 18320−18326

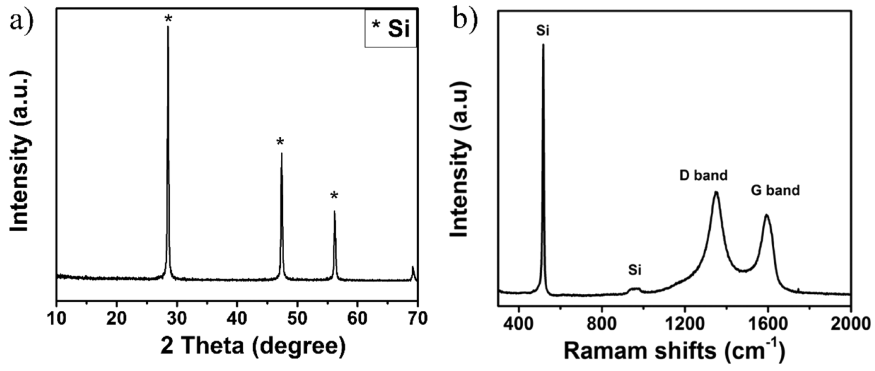

Figure 3. (a) XRD pattern and (b) Ramam spectra of the G@Si@G films.

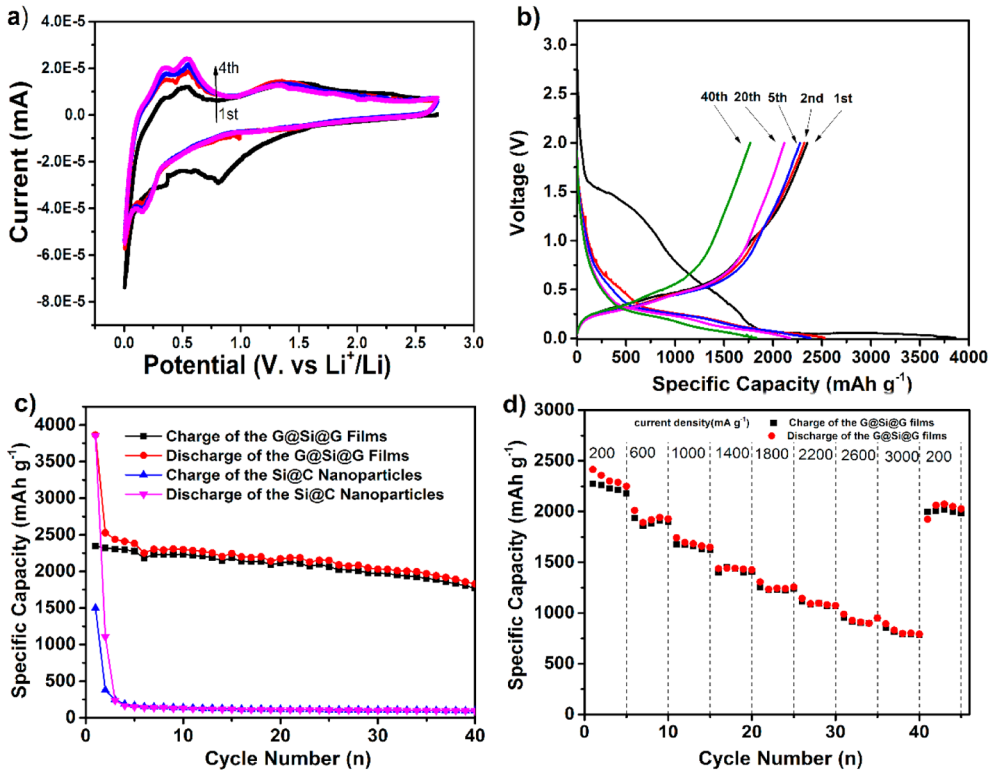

Figure 4. (a) Cyclic voltammograms of the G@Si@G hybrid films at a scan rate of 0.04 mV s^{-1} in the voltage range from 0.005−2.7 V. (b) Voltage profiles of the G@Si@Gfilms in the voltage range from 0.005−2 V versus Li^+/Li at a constant current density of 0.1 A g^{-1}. (c) Capacity−cycle number curves of the G@Si@G films and the Si@C NPs electrodes at a current density of 0.1 A g^{-1}; (d) the rate performances of the G@Si@G films cycled at different current densities from 0.1−3 A g^{-1}.

nanoparticles were first introduced into the GO aqueous suspensions. Then, 1 M HCl solution was employed to adjust the pH to 2. After that, ultrasonication was used to obtained stable mixed suspensions. Note that the aqueous suspension of these nanoparticles tends to sink to the bottom after a period, even after ultrasonication. After mixing with GO aqueous suspensions, the nanomaterials show good solubility. The GO sheets have lots of pi-conjugated nanopatches and hydrophobic on their surface, acting as a surfactant, which make them able to capture the nanoparticles through miscellaneous interactions (e.g., van der Waals and hydrophobic interaction) between GO and nanoparticles.[18] While Zn foils were hanged in the middle of the suspensions, surface of Zn foils were ionized by the reaction between Zn foils and the acid suspension. The GO sheets with negative charge were attracted and reduced by the Zn foils. The reaction can be described as

$$GO + Zn + H^+ \rightarrow RGO + Zn^{2+} + H_2O$$

It is noted that the Si nanoparticles (Si-NPs) were captured by the GO sheets. When the GO sheets were absorbed to the surface of the Zn foils, Si-NPs moved together with the GO sheets. After they reacted at room temperature for several hours, the Zn foils were washed with pure water to remove unreacted GO and nanoparticles. The remaining GO@Si@GO hybrid films were detached from Zn substrate by mild acid etching and followed wash by pure water. Subsequently, the detached film transformed into the well-defined G@Si@G nanosheets by annealing.

Figure 1, panel b shows the fabrication processes of the G@Si@G hybrid films. To improve the solubility and stability of commercial Si-NPs in GO solution, the Si NPs were coated by a layer of carbon (see Figure S1). While Zn foils are immersed

DOI: 10.1021/acsami.5b03942
ACS Appl. Mater. Interfaces 2015, 7, 18320−18326

in khaki suspension of GO and Si-NPs, black graphene hydrogels spontaneously grow at Zn surface. At the same time, Si-NPs were captured by the GO sheets. As shown in Figure 2, panels a and b, the surface of the free-standing G@Si@G hybrid films was porous. Si-NPs were embraced in the RGO sheets, resulting in yellow−brown sheets. Cross-sectional SEM (Figure 2c,d) of the G@Si@G hybrid films shows a uniform sandwich-like structure. The graphene sheets were interconnected in a quasiparallel manner, and the Si-NPs were loaded between the graphene sheets. As shown in Figure 2, panels e and f, every Si-NP was coated by a thin carbon layer (~5 nm), and the obtained Si/C NP was warped by the graphene sheets. The Si/C NPs had close contact with the graphene sheets. A thin layer of SiO_x was found on the surfaces of the Si NPs because of partial surface oxidation in air, as shown in the HRTEM image of Figure 2, panel f.

The carbon content of the free-standing G@Si@G film was determined to be ~50.8 wt % from the TGA profile shown in Figure S2. Figure 3, panel a shows the XRD pattern of the G@Si@G film in which all of the XRD peaks agree well with the standard cubic phase Si (JCPDS CARD NO 27−1402). Peaks matching up with carbon or graphene cannot be found in the XRD pattern, showing that the carbon of the as-prepared films is amorphous. Ramam spectrum was further used to characterize the G@Si@G hybrid film; peaks observed at about 517.7 and 958 cm^{-1} relate to typical Raman mode of Si. Another two broad peaks centered at 1354 cm^{-1} (D band) and 1597 cm^{-1} (G band) are indexed to the characteristic of the graphene sheets (see Figure 3b). Also, the XPS results showed GO sheets were reduced well (see Figure S3).

The cycle performance of the G@Si@G hybrid film was studied by charge/discharge galvanostatic cycles cell using Li metal as the counter electrode between 0.005 and 2 V. Figure 4, panel a shows the CV curves of the G@Si@G hybrid film. The peak observed at 0.82 V in the first discharge process disappeared in the following cycles, indicating an irreversible electrode reaction such as the formation of a solid electrolyte interphase (SEI) layer.[2] Two anodic peaks at ~0.34 and 0.5 V in the first oxidation process can be put down as the reaction from Li_xSi to Si.[19] After the first cycle, another two cathodic peaks at ~0.2 and 0.01 V indicated the forming of some different Li−Si phase during electrochemical lithiation.[20] Additionally, owing to the formation of SEI and the local structure rearrangement of the electrode during electrochemical reaction, the first cycle's curve showed much difference with the latter cycle's curves.[21]

Figure 4, panel b shows the voltage profiles of the G@Si@G hybrid film at a current density of 100 mA g^{-1}. The G@Si@G film exhibits the typical charge/discharge profiles of the Si electrode. The initial discharge and charge capacities of the G@Si@G film are 3865 and 2345 mA h g^{-1}, respectively. Note that the capacity was calculated based on the total mass of composite film so that it consists of the weight of Si, carbon coating layer, and graphene sheets. Some reactions such as the irreversible reaction of silicon with Li, the irreversible capacity of amorphous carbon, and the formation of SEI layers could contribute to the large initial discharge capacity of the electrode.[22−25] This reaction may result in the capacity fade due to direct contact between the high-surface-area graphene sheets and the electrolyte.[26,27] After the first cycle, the columbic efficiency is significantly improved, reaching ~97%.[20,25]

Figure 4, panel c compares the cyclability of G@Si@G film and Si@C NPs. For the first 10 cycles, the specific capacity of the G@Si@G film is as high as 2200 mA h g^{-1}. Even after 40 cycles, it still delivers a reversible capacity of ~1800 mA h g^{-1} at a current density of 100 mA g^{-1}. The capacity loss between the second and 40th cycle is about 20%, demonstrating the excellent cyclability of G@Si@G. In the case of the electrode made of the Si@C NPs, it only showed a reversible capacity (~1200 mA h g^{-1}) in the first several cycles, which decreased dramatically later owing to the separation of active materials. The enhanced electrochemical performance of the G@Si@G films demonstrated that 3D graphene-based sandwich architecture offers a buffer cushion to accommodate the huge volume expansion during alloying/dealloying.[21,28] Moreover, the G@Si@G films with higher weight ratio of Si (H-G@Si@G) were obtained by increasing the mass of Si-NPs. The H-G@Si@G films showed worse electrochemical performance (see Figure S4) due to larger volume change of Si when cycling.

The rate performance of G@Si@G electrode was further inspected (see Figure 4d). The G@Si@G films can exhibit a reversible capacity of 2275, 1934, 1679, 1454, 1253, 1111, 954, and 851 mA h g^{-1} at current densities of 200, 600, 1000, 1400, 1800, 2200, 2600, and 3200 mA g^{-1}, respectively. The specific capacity can recover to 2000 mA h g^{-1} when the current density is tuned back to 200 m A g^{-1}, implying the good reversibility and stability of the G@Si@G films. As far as the long-term stability of the G@Si@G anode is concerned, a cycling test for 400 cycles at a current density of 1000 mA g^{-1} was carried out. Figure 5 reveals that an electrode capacity of

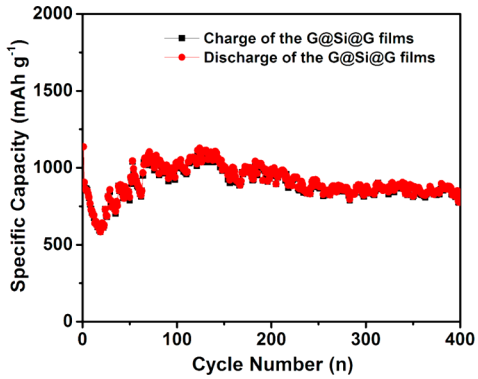

Figure 5. Long-term capability test for the G@Si@G films at 1 A g^{-1} for 400 cycles, which were activated first for three cycles at a small current density of 100 mA g^{1}.

approximately 816 mA h g^{-1} was still obtained after 400 cycles. Interestingly, the capacity of G@Si@G anode decreases during the first 40 charging/discharging cycles, and then it increases gradually. The continuous increase in G@Si@G may be put down to the tight graphene structure, which can hold the Si nanoparticles with large volume change during repeated cycling, thus increasing the amount of active Si accessible by electrolytes, which is reported in previous literature.[29] The enhanced Li storage performance of G@Si@G can result from the synergistic effects of carbon-coated Si, and the graphene sheets associated with a unique 3D sandwich structure (i) enhanced electrical conductivity due to the use of both graphene and carbon shell, thus enhancing the rate performance. (ii) The carbon coated on the surface of active materials particles can enhance the structural stability through suppressing the clustering of Si nanoparticles during the cycling. (iii) The Si-NPs sandwiched between the graphene sheets not only afford a stretchy cushion to accommodate the volume

DOI: 10.1021/acsami.5b03942
ACS Appl. Mater. Interfaces 2015, 7, 18320−18326

expansion during cycling, but also supply close interaction between nanoparticles and graphene substrate, as demonstrated in Figure 6, panel a.[23,308] The electrochemical performance of

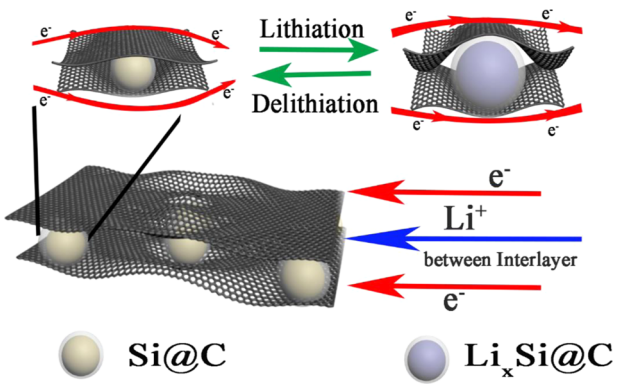

Figure 6. Schematic representation of the electrochemical reaction path of G@Si@G films.

the current work is also compared with other graphene-Si nanocomposite electrodes reported in the literature (see Supporting Information Table S1). By comparison, the G@Si@G films show improved lithium storage properties.

To further demonstrate the general strategy of this sandwich design, sandwich structure G@Fe_2O_3@G and G@TiO_2@G film was also prepared (see Figure S5). Figure S6 displays the electrochemical performance of the G@Fe_2O_3@G film electrode. After 100 cycles at the current density of 200 mA g^{-1}, the G@Fe_2O_3@G electrode delivered a reversible capacity of 1200 mA h g^{-1}. Even cycled at the high current density (1000 mA g^{-1}), the capacity of the electrodes remained on a high value of ~620 mA h g^{-1}, thus showing its high electrochemical performance. For the G@TiO_2@G, cycling at the current density of 1000 mA g^{-1}, the electrode exhibits a capacity of ~100 mA h g^{-1}after 100 cycles (see Figure S7). The improved electrochemical performance is believed to result from the unique features of the sandwich structure of graphene paper and electroactive materials.

4. CONCLUSIONS

In conclusion, a general strategy for the fabrication of sandwich-like graphene-based hybrid films through interfacial electroless reduction of GO has been developed. This facile method is effective in fabricating the 3D graphene frameworks with nanoparticles decorated between the layers of graphene. The optimum design of sandwich structure reduces the electronic transport length, suppresses the agglomeration of electroactive materials, and offers a flexible matrix to buffer the volume expansion during cycling. Additionally, the porous sandwich structure consisting of platelike graphene with large surface area provides effective electrolyte infiltration and promotes diffusion rate of Li^+, which lead to an improved rate capability. The approach reported here has easy scalability for industrial application, and the 3D graphene-based hybrid films can be further exploited for other applications such as catalysis and supercapacitors.

ASSOCIATED CONTENT

Supporting Information

The Supporting Information is available free of charge on the ACS Publications website at DOI: 10.1021/acsami.5b03942.

Characterization and electrochemical performance of as-prepared materials (PDF)

AUTHOR INFORMATION

Corresponding Author

*E-mail: yanyumse@ustc.edu.cn.

Notes

The authors declare no competing financial interest.

ACKNOWLEDGMENTS

This work was financially supported by the National Natural Science Foundation of China (Nos. 21171015 and 21373195), the "Recruitment Program of Global Experts", the program for New Century Excellent Talents in University (NCET-12-0515), the Fundamental Research Funds for the Central Universities (WK2060140014, WK2060140016), and the Collaborative Innovation Center of Suzhou Nano Science and Technology.

REFERENCES

(1) Tarascon, J. M.; Armand, M. Issues and challenges Facing Rechargeable Lithium Batteries. *Nature* **2001**, *414* (6861), 359−367.
(2) Yu, Y.; Gu, L.; Zhu, C. B.; Tsukimoto, S.; van Aken, P. A.; Maier, J. Reversible Storage of Lithium in Silver-Coated Three-Dimensional Macroporous Silicon. *Adv. Mater.* **2010**, *22* (20), 2247−2250.
(3) Hu, L.; Wu, H.; Gao, Y.; Cao, A.; Li, H.; McDough, J.; Xie, X.; Zhou, M.; Cui, Y. Silicon−Carbon Nanotube Coaxial Sponge as Li-Ion Anodes with High Areal Capacity. *Adv. Energy. Mater.* **2011**, *1* (4), 523−527.
(4) Tarascon, J. M.; Poizot, P.; Laruelle, S.; Grugeon, S.; Dupont, L. Nano-Sized Transition-Metal Oxides as Negative-Electrode Materials for Lithium-Ion Batteries. *Nature* **2000**, *407* (6803), 496−499.
(5) Liu, X. H.; Zhong, L.; Huang, S.; Mao, S. X.; Zhu, T.; Huang, J. Y. Size-Dependent Fracture of Silicon Nanoparticles During Lithiation. *ACS Nano* **2012**, *6* (2), 1522−1531.
(6) Cheng, J. S.; Du, J. Facile Synthesis of Germanium-Graphene Nanocomposites and Their Application as Anode Materials for Lithium Ion Batteries. *CrystEngComm* **2012**, *14* (2), 397−400.
(7) Wang, X.; Cao, X. Q.; Bourgeois, L.; Guan, H.; Chen, S. M.; Zhong, Y. T.; Tang, D. M.; Li, H. Q.; Zhai, T. Y.; Li, L.; Bando, Y.; Golberg, D. N-Doped Graphene-SnO2 Sandwich Paper for High-Performance Lithium-Ion Batteries. *Adv. Funct. Mater.* **2012**, *22* (13), 2682−2690.
(8) Wang, B.; Li, X.; Luo, B.; Hao, L.; Zhou, M.; Zhang, X.; Fan, Z.; Zhi, L. Approaching the Downsizing Limit of Silicon for Surface-Controlled Lithium Storage. *Adv. Mater.* **2015**, *27* (9), 1526−1532.
(9) Ngo, D. T.; Kalubarme, R. S.; Le, H. T. T.; Fisher, J. G.; Park, C.-N.; Kim, I.-D.; Park, C.-J. Carbon-Interconnected Ge Nanocrystals as an Anode with Ultra-Long-Term Cyclability for Lithium Ion Batteries. *Adv. Funct. Mater.* **2014**, *24* (33), 5291−5298.
(10) Wu, Z. S.; Zhou, G. M.; Yin, L. C.; Ren, W.; Li, F.; Cheng, H. M. Graphene/Metal Oxide Composite Electrode Materials for Energy Storage. *Nano Energy* **2012**, *1* (1), 107−131.
(11) Zhang, B. A.; Zheng, Q. B.; Huang, Z. D.; Oh, S. W.; Kim, J. K. Sno2-Graphene-Carbon Nanotube Mixture for Anode Material with Improved Rate Capacities. *Carbon* **2011**, *49* (13), 4524−4534.
(12) Zhang, C. F.; Peng, X.; Guo, Z. P.; Cai, C. B.; Chen, Z. X.; Wexler, D.; Li, S.; Liu, H. K. Carbon-Coated Sno2/Graphene Nanosheets as Highly Reversible Anode Materials for Lithium Ion Batteries. *Carbon* **2012**, *50* (5), 1897−1903.
(13) Li, D.; Seng, K. H.; Shi, D. Q.; Chen, Z. X.; Liu, H. K.; Guo, Z. P. A Unique Sandwich-Structured C/Ge/Graphene Nanocomposite as An Anode Material for High Power Lithium Ion Batteries. *J. Mater. Chem. A* **2013**, *1* (45), 14115−14121.
(14) Zhao, L.; Gao, M. M.; Yue, W. B.; Jiang, Y.; Wang, Y.; Ren, Y.; Hu, F. Q. Sandwich-Structured Graphene-Fe3O4@Carbon Nano-

composites for High-Performance Lithium-Ion Batteries. *ACS Appl. Mater. Interfaces* **2015**, *7* (18), 9709−9715.
(15) Yue, W. B.; Jiang, S. H.; Huang, W. J.; Gao, Z. Q.; Li, J.; Ren, Y.; Zhao, X. H.; Yang, X. J. Sandwich-Structural Graphene-Based Metal Oxides as Anode Materials for Lithium-Ion Batteries. *J. Mater. Chem. A* **2013**, *1* (23), 6928−6933.
(16) Ji, J.; Ji, H.; Zhang, L. L.; Zhao, X.; Bai, X.; Fan, X.; Zhang, F.; Ruoff, R. S. Graphene-Encapsulated Si on Ultrathin-Graphite Foam as Anode for High Capacity Lithium-Ion Batteries. *Adv. Mater.* **2013**, *25* (33), 4673−4677.
(17) Yang, Y.; Ma, H.; Zhuang, J.; Wang, X. Morphology-Controlled Synthesis of Hematite Nanocrystals and Their Facet Effects on Gas-Sensing Properties. *Inorg. Chem.* **2011**, *50* (20), 10143−10151.
(18) Cote, L. J.; Kim, J.; Tung, V. C.; Luo, J. Y.; Kim, F.; Huang, J. X. Graphene Oxide as Surfactant Sheets. *Pure Appl. Chem.* **2010**, *83* (1), 95−110.
(19) Zhou, X. S.; Yin, Y. X.; Wan, L. J.; Guo, Y. G. Self-Assembled Nanocomposite of Silicon Nanoparticles Encapsulated in Graphene through Electrostatic Attraction for Lithium-Ion Batteries. *Adv. Energy. Mater.* **2012**, *2* (9), 1086−1090.
(20) Wu, Z.-S.; Ren, W.; Xu, L.; Li, F.; Cheng, H.-M. Doped Graphene Sheets As Anode Materials with Superhigh Rate and Large Capacity for Lithium Ion Batteries. *ACS Nano* **2011**, *5* (7), 5463−5471.
(21) Zhou, X. S.; Yin, Y. X.; Wan, L. J.; Guo, Y. G. Facile Synthesis of Silicon Nanoparticles Inserted into Graphene Sheets as Improved Anode Materials for Lithium-Ion Batteries. *Chem. Commun.* **2012**, *48* (16), 2198−2200.
(22) Nguyen, B. P. N.; Kumar, N. A.; Gaubicher, J.; Duclairoir, F.; Brousse, T.; Crosnier, O.; Dubois, L.; Bidan, G.; Guyomard, D.; Lestriez, B. Nanosilicon-Based Thick Negative Composite Electrodes for Lithium Batteries with Graphene as Conductive Additive. *Adv. Energy. Mater.* **2013**, *3* (10), 1351−1357.
(23) Chae, C.; Noh, H.-J.; Lee, J. K.; Scrosati, B.; Sun, Y.-K. A High-Energy Li-Ion Battery Using a Silicon-Based Anode and a Nano-Structured Layered Composite Cathode. *Adv. Funct. Mater.* **2014**, *24* (20), 3036−3042.
(24) Yu, Y.; Gu, L.; Lang, X. Y.; Zhu, C. B.; Fujita, T.; Chen, M. W.; Maier, J. Li Storage in 3D Nanoporous Au-Supported Nanocrystalline Tin. *Adv. Mater.* **2011**, *23* (21), 2443−2447.
(25) Xu, Y. H.; Zhu, Y. J.; Han, F. D.; Luo, C.; Wang, C. S. 3D Si/C Fiber Paper Electrodes Fabricated Using a Combined Electrospray/Electrospinning Technique for Li-Ion Batteries. *Adv. Energy. Mater.* **2015**, *5*, 1400753.
(26) Xue, D.-J.; Xin, S.; Yan, Y.; Jiang, K.-C.; Yin, Y.-X.; Guo, Y.-G.; Wan, L.-J. Improving the Electrode Performance of Ge through Ge@C Core−Shell Nanoparticles and Graphene Networks. *J. Am. Chem. Soc.* **2012**, *134* (5), 2512−2515.
(27) Hu, Y.-S.; Demir-Cakan, R.; Titirici, M.-M.; Müller, J.-O.; Schlögl, R.; Antonietti, M.; Maier, J. Superior Storage Performance of a Si@SiOx/C Nanocomposite as Anode Material for Lithium-Ion Batteries. *Angew. Chem., Int. Ed.* **2008**, *47* (9), 1645−1649.
(28) Ren, J. G.; Wu, Q. H.; Tang, H.; Hong, G.; Zhang, W. J.; Lee, S. T. Germanium-Graphene Composite Anode for High-Energy Lithium Batteries with Long Cycle Life. *J. Mater. Chem. A* **2013**, *1* (5), 1821−1826.
(29) Wang, X.; Cao, X.; Bourgeois, L.; Guan, H.; Chen, S.; Zhong, Y.; Tang, D.-M.; Li, H.; Zhai, T.; Li, L.; Bando, Y.; Golberg, D. N-Doped Graphene-SnO2 Sandwich Paper for High-Performance Lithium-Ion Batteries. *Adv. Funct. Mater.* **2012**, *22* (13), 2682−2690.
(30) Evanoff, K.; Magasinski, A.; Yang, J. B.; Yushin, G. Nanosilicon-Coated Graphene Granules as Anodes for Li-Ion Batteries. *Adv. Energy. Mater.* **2011**, *1* (4), 495−498.

DOI: 10.1021/acsami.5b03942
ACS Appl. Mater. Interfaces 2015, 7, 18320−18326